Landau-Ginzburg model of interphase boundaries in improper ferroelastic Perovskites of D_{4h}^{18} symmetry

Wenwu Cao* and Gerhard R. Barsch
Materials Research Laboratory and Department of Physics, The Pennsylvania State University, University Park, Pennsylvania 16802
(Received 7 August 1989; revised manuscript received 2 October 1989)

The Landau model of Slonczewski and Thomas (1970) for the improper ferroelastic O_h^1-D_{4h}^{18} phase transition in perovskite-structure compounds has been extended by including spatial gradient terms of the three-component primary order parameter (OP) and applied to calculate the OP profile and the strain distribution for antiphase and for twin boundaries in the tetragonal phase. In order to obtain quasi-one-dimensional kink-type solitary-wave solutions for which the OP and the strain depend only on the coordinate normal to the interface plane, lateral surface forces are required which allow for the shape change associated with ferroelastic interfaces, but which prevent expansion or contraction within the boundary plane. Numerical application to $SrTiO_3$, including calculation of the thickness and energy of both types of interphase boundaries versus temperature, is also presented.

I. INTRODUCTION

Strontium titanate[1] ($SrTiO_3$) and several fluoroperovskites[2–5] undergo a nearly continuous improper ferroelastic phase transition[6] from the high-temperature cubic (O_h^1) to the low-temperature tetragonal (D_{4h}^{18}) perovskite structure (composition ABX_3). This transition is driven by the softening of a degenerate-zone corner (R_{25}) phonon mode[7] that consists of the antiphase rotations of adjacent (nearly rigid) BX_6 octahedra around any of the three cubic axes of the cubic prototype phase, resulting in a quadrupling of the crystallographic unit cell and the concomitant loss of cubic symmetry[8] (Fig. 1). In addition, the transition is accompanied by a spontaneous strain, consisting of a (nearly) volume conserving deviatoric deformation of the tetragonal unit cell[8] that is induced by a nonlinear ("rotostrictive") coupling between the rotation and the strain.[9,10]

Thomas and Müller[9] have described this transition (together with the zone corner mode-driven cubic-trigonal transition occurring in other perovskites) within the framework of the Landau theory of continuous phase transitions. In this theory the three components Q_i ($i=1,2,3$) of the *primary* order parameter (OP) were taken as the displacements of the X ions that are related to the rotation angles ϕ_i of the BX_6 octahedra according to[9] $Q_i=(a/2)\tan\phi_i$ (a denotes a lattice constant; Fig. 1). Subsequently Slonczewski and Thomas[10] (ST) have accounted for the *induced* spontaneous tetragonal deformation by including the coupling between the primary OP and the components of the elastic strain tensor[11] $\eta_{ij}=\frac{1}{2}(u_{ij}+u_{j,i})$ that take on the role of a *secondary* (multicomponent) OP.

In the tetragonal phase three orientation states, or *variants*, occur; they correspond to the three possible directions that the rotation axis, or the (parallel) tetragonal axis, may assume along any of the three cubic axes. Adjacent domains consisting of different tetragonal variants may be separated from each other by two types of interphase boundaries: twin boundaries (TB's) or ferroelastic domain walls, and antiphase boundaries (APB's). The former separate different domains consisting of different tetragonal variants and can be observed by optical methods.[12] The latter represent interfaces between domains with the same direction of the tetragonal and rotation axis, but with the sequence of the rotation angles of alternating signs along the rotation axis reversed [Fig. 1(c)]. Coherent interphase boundaries are planar and are characterized by their orientation, by the order-parameter profile along the direction of their normal (i.e. their thickness or width), and by their interfacial energy. The orientation and energy (in conjunction with proper boundary conditions) determine the morphology of the domain structure. The width affects the wall mobility and the applicability of continuum theoretical models to interface boundaries, with wider boundaries being more

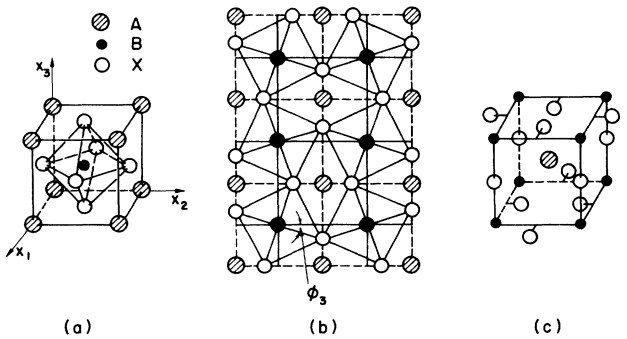

FIG. 1. The O_h-D_{4h} transformation in the perovskite structure (after Unoki and Sakudo[8]): (a) Unit cell of the cubic parent phase. (b) The plane $X_3=a/2$ for the variant of the tetragonal product phase with rotations of the BX_6-octahedra around the X_3 axis. (c) Displacement pattern of the X ions with respect to a unit cell shifted by $(a/2)$ [111], showing that BX_6 octahedra in successive (001) layers rotate in opposite directions.

mobile and more amenable to continuum theoretical modeling. The interfacial orientation can be explained theoretically on the basis of the strain compatibility between adjacent domains[13–15] or, more generally, from group theoretical compatibility relations.[16,17] By means of diffraction contrast and high-resolution transmission electron microscopy, it has been shown that, in general, TB's are at most only a few lattice constant wide, and that APB's are atomically sharp.[13] However, as expected on theoretical grounds, for second-order transitions it has been found that the width increases sharply as the transition temperature is approached from below,[13] as most directly measured for ferroelectric potassium dihydrogen phosphate (KDP) by x-ray diffraction.[18] The energy of interphase boundaries is difficult to measure directly; thus experimental data on this quantity and its temperature dependence are sparse and uncertain.

Theoretical models for interphase boundaries in ferroic materials were inspired by the Landau-Ginzburg theory of ferromagnetic Bloch walls[19] and have been proposed so far only for improper ferroelastics that are either proper ferroelectrics[20,21] or improper ferroelectrics (as in Gadolinium molybdate[22–24]), and for proper ferroelastics.[25–28] In all these models the OP profile is given by a solitary-wave solution of a phenomenological (continuum theoretical) energy functional, which includes (local) nonlinear terms in the OP that allow for multivalued solutions for the OP corresponding to the different orientation states in the homogeneous phase, plus (nonlocal) gradient terms for the OP in the harmonic approximation, which determine the width and energy of the interface.

In this paper we present a continuum theoretical model for TB's and APB's in the tetragonal (D_{4h}^{18}) phase of perovskites, which results from the improper ferroelastic transition from the cubic (O_h^1) prototype phase that is driven by the softening of the R_{25} mode. This model is an extension of the Landau model of Slonczewski and Thomas[10] pertaining to the transition of the *homogeneous* phase and is obtained by adding the symmetry-allowed rotation gradient terms to their free energy. These terms account for the energy associated with differences in the rotation angle between adjacent (pairs of) BX_6 octahedra. Whereas numerical application of previous Landau-Ginzburg models to specific materials was hampered by lack of a procedure for relating the gradient coefficients to independent experimental data, we will show in the Appendix how the rotation gradient terms of our model may be determined from the anisotropic dispersion of the soft R_{25} phonon mode in the vicinity of the Brillouin-zone corner. These results will allow us to include in the following a numerical application of our model to $SrTiO_3$.

Apart from their crystallographic interest, ferroelastic TB's are important because they affect the propagation of acoustic waves,[29,30] phonon dispersion,[31] as well as thermal properties and the electron-phonon interaction.[32] Furthermore, ferroelastic TB's have been observed in the perovskite-based high-T_c oxide superconductors of the K_2NiO_4 structure[33] and of the $YBa_2Cu_3O_{7-x}$ type,[34,35] and they result from a tetragonal-orthorhombic improper ferroelastic transition.[36,37] For La_2CuO_4 this transition is driven by a soft zone-edge phonon mode with wave vector[38] $k=(\pi/a)(1,1,0)$ so that a Ginzburg-Landau model for interphase boundaries in 2:1:4 superconductors may be constructed in a manner very similar to that in this paper. However, for the 1:2:3 superconductors the tetragonal-orthorhombic transition is associated with the ordering of oxygen ions along the chains in the crystallographic b direction.[39] Thus, for this case our model of TB's in perovskites would have to be adapted and augmented by inclusion of other (diffusive) degrees of freedom.[40,41]

This paper is organized as follows. In Sec. II we discuss the theoretical model and review the application to the homogeneously transformed tetragonal phase,[10] in Secs. III and IV we present the static solitary-wave solutions for APB's and TB's respectively, and in Sec. V numerical application to $SrTiO_3$ is made. Sections VI and VII contain a discussion and a concluding summary, respectively.

II. THEORETICAL MODEL

A. Landau-Ginzburg free energy

The (rotationally invariant) Landau-Ginzburg free energy (LGFE) density, which describes the second-order transitions of the cubic perovskite structure that are driven by the softening of the R_{25} zone corner mode, is to lowest order given by

$$F(Q_i,Q_{i,j}\eta_{kl})=F_L(Q_i)+F_{\rm el}(\eta_{kl})+F_c(Q_i,\eta_{kl})+F_G(Q_{i,j})\ . \tag{2.1}$$

Here F_L is the Landau free-energy density for the primary OP $\mathbf{Q}=\{Q_i\}$ $(i=1,2,3)$,

$$F_L=\tfrac{1}{2}K(Q_1^2+Q_2^2+Q_3^2)+A(Q_1^2+Q_2^2+Q_3^2)^2+A_n(Q_1^2Q_2^2+Q_1^2Q_3^2+Q_2^2Q_3^2)\ ; \tag{2.2}$$

$$F_{\rm el}=\tfrac{1}{2}c_{11}(\eta_{11}^2+\eta_{22}^2+\eta_{33}^2)+c_{12}(\eta_{11}\eta_{22}+\eta_{11}\eta_{33}+\eta_{22}\eta_{33})+2c_{44}(\eta_{12}^2+\eta_{13}^2+\eta_{23}^2) \tag{2.3}$$

is the elastic energy density in the harmonic approximation;

$$F_c=-B_1(\eta_{11}Q_1^2+\eta_{22}Q_2^2+\eta_{33}Q_3^2)-B_2[\eta_{11}(Q_2^2+Q_3^2)+\eta_{22}(Q_1^2+Q_3^2)+\eta_{33}(Q_1^2+Q_2^2)]-2B_t(\eta_{12}Q_1Q_2+\eta_{13}Q_1Q_3+\eta_{23}Q_2Q_3) \tag{2.4}$$

is the coupling energy between the primary OP and the strain $\eta=\{\eta_{ij}\}$ $(i,j=1,2,3)$; and

$$F_G=\tfrac{1}{2}D_{11}(Q_{1,1}^2+Q_{2,2}^2+Q_{3,3}^2)+D_{12}(Q_{1,1}Q_{2,2}+Q_{1,1}Q_{3,3}+Q_{2,2}Q_{3,3})+\tfrac{1}{2}D_{44}[(Q_{1,2}+Q_{2,1})^2+(Q_{1,3}+Q_{3,1})^2+(Q_{2,3}+Q_{3,2})^2] \tag{2.5}$$

is the gradient energy for the primary OP pertaining to spatially inhomogeneous configurations, where indices (i) preceded by a comma denote differentiation with respect to the position coordinates X_i.

The LGFE, Eq. (2.1) is obtained from the Landau free energy for the homogeneous phase (which equals $F_L+F_{el}+F_c$) as introduced by Slonczewski and Thomas[10] by adding the OP gradient contribution, Eq. (2.5). All expansion coefficients in Eqs. (2.2) to (2.5) are referred to the cubic parent phase; they are given here in the notation and with the same meaning as used by Slonczewski and Thomas,[10] except that the η_{ij} are the components of the linear strain *tensor* (i.e., they include, as shown, a factor $\frac{1}{2}$ for the off-diagonal elements). The three (rotation) gradient coefficients D_{11}, D_{12}, and D_{44}, given here also in Voigt notation, are determined by the anisotropy of the dispersion of the soft R_{25} phonon mode in the vicinity of the Brillouin-zone corner.

For treating the OP-strain coupling it is convenient to introduce the following symmetry coordinates:

$$\begin{bmatrix} P_1 \\ P_2 \\ P_3 \end{bmatrix} = \mathbf{S} \begin{bmatrix} Q_1^2 \\ Q_2^2 \\ Q_3^2 \end{bmatrix} , \tag{2.6a}$$

$$P_4=2Q_2Q_3,\quad P_5=2Q_1Q_3,\quad P_6=2Q_1Q_2 , \tag{2.6b}$$

$$\begin{bmatrix} e_1 \\ e_2 \\ e_3 \end{bmatrix} = \mathbf{S} \begin{bmatrix} \eta_{11} \\ \eta_{22} \\ \eta_{33} \end{bmatrix} , \tag{2.7a}$$

$$e_4=2\eta_{23},\quad e_5=2\eta_{13},\quad e_6=2\eta_{12} , \tag{2.7b}$$

where

$$\mathbf{S}=\begin{bmatrix} \frac{1}{\sqrt{3}} & \frac{1}{\sqrt{3}} & \frac{1}{\sqrt{3}} \\ \frac{1}{\sqrt{2}} & -\frac{1}{\sqrt{2}} & 0 \\ \frac{1}{\sqrt{6}} & \frac{1}{\sqrt{6}} & -\frac{2}{\sqrt{6}} \end{bmatrix} . \tag{2.8}$$

Then the elastic and the coupling energies, Eqs. (2.3) and (2.4), become, respectively,

$$F_{el}=\tfrac{1}{2}\sum_{\alpha=1}^{6}\hat{c}_{\alpha\alpha}e_\alpha^2 , \tag{2.9}$$

$$F_c=-\sum_{\alpha=1}^{6}\hat{B}_{\alpha\alpha}e_\alpha P_\alpha . \tag{2.10}$$

Here

$$\hat{c}_{11}=c_{11}+2c_{12} , \tag{2.11a}$$

$$\hat{c}_{22}=\hat{c}_{33}=c_{11}-c_{12} , \tag{2.11b}$$

$$\hat{c}_{44}=\hat{c}_{55}=\hat{c}_{66}=c_{44} , \tag{2.11c}$$

are the elastic constant eigenvalues for cubic symmetry and are (proportional to or equal to) the bulk modulus and the two shear moduli. Furthermore,

$$\hat{B}_{11}=B_1+2B_2 , \tag{2.12a}$$

$$\hat{B}_{22}=\hat{B}_{33}=B_1-B_2 , \tag{2.12b}$$

$$\hat{B}_{44}=\hat{B}_{55}=\hat{B}_{66}=\tfrac{1}{2}B_t . \tag{2.12c}$$

B. Equilibrium conditions

From the variational derivative of the total energy

$$\delta\int\int\int F(Q_i,Q_{i,j},\eta_{kl})dx_1dx_2dx_3=0 , \tag{2.13}$$

one obtains the following six static equilibrium conditions (summation convention):

$$\frac{\partial}{\partial x_j}\left[\frac{\partial F}{\partial Q_{i,j}}\right]-\frac{\partial F}{\partial Q_i}=0\quad (i,j=1,2,3) , \tag{2.14}$$

$$\sigma_{ij,j}^{tot}=0\quad (i,j=1,2,3) . \tag{2.15}$$

Here

$$\sigma_{ij}^{tot}=\frac{\partial F}{\partial\eta_{ij}}=\frac{\partial F_{el}}{\partial\eta_{ij}}+\frac{\partial F_c}{\partial\eta_{ij}} \tag{2.16}$$

represents the total Cauchy stress tensor; its two contributions arise from the purely harmonic elastic response of the crystal, plus an anharmonic term from the coupling of the strain to the primary OP.

The six coupled partial differential equations (2.14) and (2.15) plus boundary conditions determine the two sets of field variables $Q_i(\mathbf{x})$ and $u_i(\mathbf{x})$. In the following, after recalling the solutions of Slonczewski and Thomas[10] pertaining to the *homogeneous* product phase, we will give special solutions that describe APB's and TB's.

C. Homogeneous phase

In the homogeneous state the OP and the strain are constant, so that

$$Q_{i,j}=0 , \tag{2.17a}$$

$$u_{k,lm}=0 . \tag{2.17b}$$

Then Eqs. (2.14) and (2.15) reduce respectively, to

$$\frac{\partial F}{\partial Q_i}=0 , \tag{2.18a}$$

$$\sigma_{ij}^{tot}=\text{const} . \tag{2.18b}$$

For $K>0$ and $\sigma_{ij}^{tot}=0$ the equilibrium state corresponds to the cubic high-temperature phase[9,10] $\mathbf{Q}=\mathbf{0}$, $\eta=0$.

In the low-temperature regime $K<0$ for vanishing total stress, $\sigma_{ij}^{tot}=0$ one obtains from Eqs. (2.16) and (2.7)–(2.10) the induced spontaneous strain as

$$e_\alpha=(\hat{B}_{\alpha\alpha}/\hat{c}_{\alpha\alpha})P_\alpha . \tag{2.19}$$

Inserting this result into Eqs. (2.9) and (2.10) one obtains in view of Eqs. (2.1) and (2.2) the effective Landau free energy[10]

$$F_{L,\text{eff}}=(K/2)(Q_1^2+Q_2^2+Q_3^2)+A'(Q_1^2+Q_2^2+Q_3^2)^2+A_n'(Q_1^2Q_2^2+Q_1^2Q_3^2+Q_2^2Q_3^2) \quad (2.20)$$

with the renormalized anharmonic expansion coefficients[10]

$$A'=A-\frac{\hat{B}_{11}^2}{6\hat{c}_{11}}-\frac{\hat{B}_{22}^2}{3\hat{c}_{22}}, \quad (2.21a)$$

$$A_n'=A_n+\frac{\hat{B}_{22}^2}{\hat{c}_{22}}-\frac{2\hat{B}_{44}^2}{\hat{c}_{44}}. \quad (2.21b)$$

The possible solutions of Eq. (2.18a) depend on these coefficients as shown in the phase diagram[9,10] of Fig. 2. The solutions for the tetragonal and for the trigonal phase then become, respectively,[10]

$$Q=(\pm Q_0,0,0),(0,\pm Q_0,0),(0,0,\pm Q_0), \quad (2.22)$$

$$Q=(\pm Q_0,\pm Q_0,\pm Q_0)/\sqrt{3}, \quad (2.23)$$

where for the tetragonal phase

$$Q_0=(-K/4A')^{1/2}. \quad (2.24)$$

The different signs in Eq. (2.22), and their different combinations in Eq. (2.23) describe the possible domain states (variants). For the tetragonal phase of interest here the minimum free-energy density is given by[10]

$$F_0=-K^2/16A'. \quad (2.25)$$

The components of the strain tensor parallel and perpendicular to the tetragonal axis become[10]

$$\eta_{\parallel}=(\Lambda_{11}+2\Lambda_{22})Q_0^2/3, \quad (2.26a)$$

$$\eta_{\perp}=(\Lambda_{11}-\Lambda_2)Q_0^2/3, \quad (2.26b)$$

where

$$\Lambda_{\alpha\alpha}=\hat{B}_{\alpha\alpha}/\hat{c}_{\alpha\alpha} \quad (2.27)$$

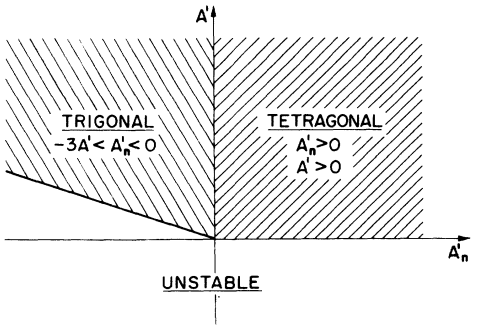

FIG. 2. Phase diagram for the D_{4h} and D_{3h} perovskite product phases in terms of the anharmonic parameters A' and A_n' [after Thomas and Müller (Ref. 9)].

For later reference these results are summarized in Table I.

III. ANTIPHASE BOUNDARY

In the tetragonal perovskite phase as shown in Fig. 1(c) adjacent octahedra lying on the same rotation axis (x_3) alternate in the sign of the rotation angle. Because of the weak coupling of the octahedra along the rotation axis, this sequence can be reversed in some part of the crystal, thereby creating an APB perpendicular to the rotation axis. In order to make contact with the atomistic lattice dynamical description, we consider the vertical row of X ions passing through the front face of the unit cell in Fig. 1(a) with position coordinates $\mathbf{x}(n_3)=(1,\frac{1}{2},\frac{1}{2}+n_3)a$, where the integer n_3 labels the unit cells along x_3, and $n_3=0$ refers to the unit cell in Fig. 1(a). Assuming a clockwise rotation of the BX_6 octahedron in Fig. 1(a) around the positive x_3 direction, the displacements of the X ions considered are along x_2 and are for a *homogeneous* tetragonal phase given by [see Fig. 3(a)]

$$u_2(x_3)=Q_0\sin\frac{\pi}{a}x_3=Q_0(-1)^{n_3}. \quad (3.1)$$

TABLE I. Order parameter **Q**, strain symmetry coordinates e, and induced spontaneous strain η for the three variants of the tetragonal perovskite phase, with Q_0 and $\Lambda_{\alpha\alpha}$ given by Eqs. (2.24) and (2.27), respectively.

Tetragonal axis	**Q**	e	η
[100]	$(\pm Q_0,0,0)$	$\left[\frac{\Lambda_{11}}{\sqrt{3}},\frac{\Lambda_{22}}{\sqrt{3}},\frac{\Lambda_{22}}{\sqrt{6}},0,0,0\right]Q_0^2$	$\begin{bmatrix}\eta_{\parallel}&0&0\\0&\eta_{\perp}&0\\0&0&\eta_{\perp}\end{bmatrix}$
[010]	$(0,\pm Q_0,0)$	$\left[\frac{\Lambda_{11}}{\sqrt{3}},-\frac{\Lambda_{22}}{\sqrt{2}},\frac{\Lambda_{22}}{\sqrt{6}},0,0,0\right]Q_0^2$	$\begin{bmatrix}\eta_{\perp}&0&0\\0&\eta_{\parallel}&0\\0&0&\eta_{\perp}\end{bmatrix}$
[001]	$(0,0,\pm Q_0)$	$\left[\frac{\Lambda_{11}}{\sqrt{3}},0,-\frac{2\Lambda_{22}}{\sqrt{6}},0,0,0\right]Q_0^2$	$\begin{bmatrix}\eta_{\perp}&0&0\\0&\eta_{\perp}&0\\0&0&\eta_{\parallel}\end{bmatrix}$

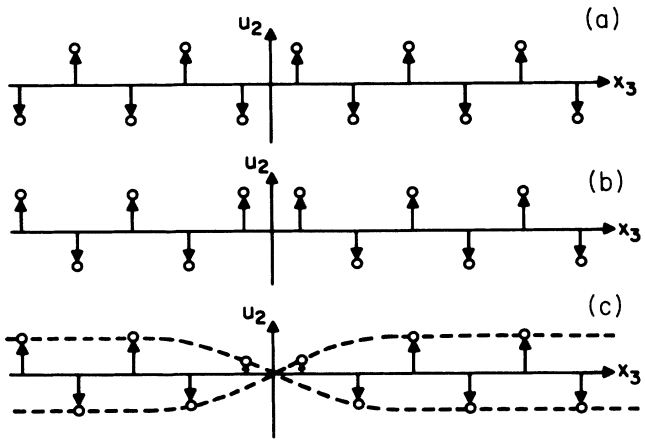

FIG. 3. Alternating displacement pattern along $x_2 \parallel$ [010] of one row of X ions parallel to x_3 passing through an ion at $\mathbf{x}=a(1,\frac{1}{2},\frac{1}{2})$ of Fig. 1(a) for $Q=(0,0,Q_3)$ (schematic). (a) Single domain tetragonal phase. (b) Discontinuous (001) antiphase boundary. (c) Continuous (001) antiphase boundary.

By reversing the sequence of rotation angles for $x_3<0$ a discontinuous (atomically sharp) APB is created, as shown in Fig. 3(b).

In order to allow for a continuous transition between the two domains $x_3 \gtrless 0$ we replace the constant amplitude Q_0 in Eq. (3.1) by a continuous function $Q_3(x_3)$ according to

$$u_2=Q_3(x_3)\sin\frac{\pi}{a}x_3 , \tag{3.2}$$

where the index 3 is now explicitly added to identify the rotation axis. By taking the OP in the form

$$\mathbf{Q}=[0,0,Q_3(x_3)] \tag{3.3}$$

the function $Q_3(x_3)$ may then be determined from the preceding equilibrium condition (2.14). Note that Eq. (3.3) results from the *assumption* that Q_3 depends on x_3 only, but that in general for a *finite* crystal, depending on the boundary conditions, Q_3 also depends on x_1 and x_2.

Because of the coupling between the OP and the strain Eq. (3.3) implies that also

$$\eta_{ij}=\eta_{ij}(x_3) , \tag{3.4a}$$

$$\sigma_{ij}=\sigma_{ij}(x_3) . \tag{3.4b}$$

Both depend only on x_3. Thus the problem considered is one dimensional (1D) in the independent variables and the OP, but 3D in stress and strain.

In order to be able to specify boundary conditions we consider a crystal in the form of a rectangular bar with dimensions $2L_1$, $2L_2$, and $2L_3$ along x_1, x_2, and x_3, respectively, with the tetragonal axis and (as before) the rotation axis along x_3. It turns out that for *stress-free* boundary conditions this geometry does not permit the quasi-1D solutions implied in Eqs. (3.3), (3.4a), and (3.4b). However, far away from an APB the crystal is in the homogeneous state so that for $L_3=\infty$ we may take the boundary condition

$$\lim_{x_3\to\pm\infty} Q_3(x_3)=\pm Q_0 , \tag{3.5}$$

where Q_0 is the OP for the homogeneous phase [Eq. (2.24)]. Furthermore, we may require

$$\lim_{x_3\to\pm\infty} \sigma_{ij}^{\text{tot}}(x_3)=0 \quad \text{for } ij=11,22,33 \tag{3.6a}$$

and

$$\sigma_{ij}^{\text{tot}}(x_3)\equiv 0 \quad \text{for } ij=23,13,12 . \tag{3.6b}$$

We may now proceed to deduce the boundary conditions for $\sigma_{11}(x_3)$, $\sigma_{22}(x_3)$, and $\sigma_{33}(x_3)$ that are compatible with the ansatz (3.3), (3.4a), and (3.4b).

Because of Eq. (3.3) the total LGFE (2.1) becomes explicitly, with $Q_3=Q$,

$$F=\tfrac{1}{2}KQ^2+AQ^4+\tfrac{1}{2}D_{11}Q_{,3}^2 -[B_1\eta_{33}+B_2(\eta_{11}+\eta_{22})]Q^2+F_{\text{el}} , \tag{3.7}$$

where F_{el} is given by Eq. (2.3). The components of the total stress tensor become explicitly

$$\begin{bmatrix}\sigma_{11}^{\text{tot}}\\ \sigma_{22}^{\text{tot}}\\ \sigma_{33}^{\text{tot}}\end{bmatrix}=\begin{bmatrix}c_{11} & c_{12} & c_{12}\\ c_{12} & c_{11} & c_{12}\\ c_{12} & c_{12} & c_{11}\end{bmatrix}\begin{bmatrix}\eta_{11}\\ \eta_{22}\\ \eta_{33}\end{bmatrix}-\begin{bmatrix}B_2\\ B_2\\ B_1\end{bmatrix}Q^2 , \tag{3.8a}$$

$$\sigma_{ij}^{\text{tot}}=2c_{44}\eta_{ij} \quad (ij=23,13,12) . \tag{3.8b}$$

From Eqs. (3.6b) and (3.8b) it follows that

$$\eta_{12}=\eta_{13}=\eta_{23}=0 . \tag{3.9}$$

In the absence of dislocations and disclinations the components of the strain tensor must satisfy the compatibility relations[42]

$$\eta_{22,33}+\eta_{33,22}=2\eta_{23,23} , \tag{3.10a}$$

$$\eta_{11,33}+\eta_{33,11}=2\eta_{13,13} , \tag{3.10b}$$

$$\eta_{11,22}+\eta_{22,11}=2\eta_{12,12} , \tag{3.10c}$$

$$\eta_{11,23}+\eta_{23,11}=\eta_{12,13}+\eta_{13,12} , \tag{3.10d}$$

$$\eta_{22,13}+\eta_{13,22}=\eta_{12,23}+\eta_{23,12} , \tag{3.10e}$$

$$\eta_{33,12}+\eta_{12,33}=\eta_{13,23}+\eta_{23,13} . \tag{3.10f}$$

Because of Eqs. (3.4a) and (3.9), the last four of these equations are satisfied identically; the first two may be integrated twice with the results that $\eta_{11}=\text{const}$, $\eta_{22}=\text{const}$, or

$$\eta_{11}=\eta_{11}^{\infty} , \tag{3.11a}$$

$$\eta_{22}=\eta_{22}^{\infty} . \tag{3.11b}$$

By using Eqs. (3.8a), (3.5), and (3.6a) it may be shown that at $x_3=\pm\infty$ the strain becomes equal to that of the homogeneous phase as given by Eqs. (2.26a) and (2.26b), so that

$$\eta_{11}^{\infty}=\eta_{22}^{\infty}=\eta_{\perp} , \tag{3.12a}$$

$$\eta_{33}^{\infty}=\eta_{\parallel} . \tag{3.12b}$$

The equilibrium condition (2.15) becomes

$$\sigma_{33,3}^{\mathrm{tot}}=0 . \tag{3.13}$$

In view of the boundary condition (3.6a) integration gives

$$\sigma_{33}^{\mathrm{tot}}=0 \tag{3.14a}$$

or

$$\eta_{33}(x_3)=-\frac{2c_{12}}{c_{11}}\eta_{\perp}+\frac{B_1}{c_{11}}Q^2(x_3) . \tag{3.14b}$$

The equilibrium condition (2.14) becomes

$$K^{+}Q+4A^{+}Q^3-D_{11}Q_{33}=0 , \tag{3.15}$$

where

$$K^{+}=K+\left[\frac{4B_1c_{12}}{c_{11}}-4B_2\right]\eta_{\perp} , \tag{3.16a}$$

$$A^{+}=A-\frac{B_1^2}{2c_{11}} . \tag{3.16b}$$

It can be shown that

$$\frac{K^{+}}{A^{+}}=\frac{K}{A'} . \tag{3.17}$$

Thus for $L_3=\infty$ the solution of Eq. (3.15) is a simple kink:

$$Q(x_3)=Q_0\tanh\frac{x_3}{\xi_{\mathrm{APB}}} , \tag{3.18}$$

where

$$\xi_{\mathrm{APB}}=d_{\mathrm{APB}}/2=(-2D_{11}/K^{+})^{1/2} \tag{3.19}$$

is half the thickness d_{APB} of the APB. The displacement pattern of one row of X ions through the APB as described by Eqs. (3.2) and (3.18) is illustrated in Fig. 3(c).

The only position-dependent strain component is η_{33}, which may now be written as

$$\eta_{33}(x_3)=\eta_{\parallel}-\frac{B_1}{c_{11}}Q_0^2\mathrm{sech}^2\frac{x_3}{\xi_{\mathrm{APB}}} . \tag{3.20}$$

The elastic displacement component along the tetragonal axis then becomes

$$u_3(x_3)=\eta_{\parallel}x_3-\frac{B_1}{c_{11}}Q_0^2\xi_{\mathrm{APB}}\tanh\frac{x_3}{\xi_{\mathrm{APB}}} . \tag{3.21}$$

The first term describes the displacement field for a homogeneously transformed crystal. The second term arises from the APB and corresponds to a contraction given by

$$\Delta L_3=-2\frac{B_1}{c_{11}}Q_0^2\xi_{\mathrm{APB}} . \tag{3.22}$$

Inserting Eq. (3.20) into (3.8a) gives the nonvanishing and position-dependent stress components

$$\sigma_{11}^{\mathrm{tot}}=\sigma_{22}^{\mathrm{tot}}=\left[-\frac{c_{12}}{c_{11}}B_1+B_2\right]Q_0^2\mathrm{sech}^2\frac{x_3}{\xi_{\mathrm{APB}}} . \tag{3.23}$$

Their presence is a consequence of the compatibility relations used in the derivation and arises from the requirement that the APB be free of dislocations and disclinations. Thus in order to sustain quasi-1D solutions of the form as in Eqs. (3.3), (3.4a) and (3.4b) in the presence of a defect-free APB's surface forces per unit area given by $F_1=\pm\sigma_{11}^{\mathrm{tot}}(x_3)$ and $F_2=\pm\sigma_{22}^{\mathrm{tot}}(x_3)$ must be applied perpendicular to the lateral surfaces $x_1=\pm L_1$ and $x_2=\pm L_2$, respectively, so as to constrain the crystal and keep the lateral strains η_{11} and η_{22} constant in accordance with Eqs. (3.11a), (3.11b), and (3.12a). Removal of these constraints leads to a lateral contraction or expansion of the crystal in the vicinity of the APB so that the OP and the strains also depend on the lateral variables x_1 and x_2, and the simple kink solution (3.18) is no longer valid. It should be noted, however, that for the boundary conditions (3.5), (3.6a), (3.6b), and (3.23) the preceding solution is exact and describes a fully 3D configuration with a reversal of the OP and a change of the sample dimensions along x_3.

The energy density of an APB can be obtained from

$$E_{\mathrm{APB}}=\int_{-\infty}^{+\infty}(F-F_0)dx_3 . \tag{3.24}$$

For the preceding solution, (3.18), (3.12a) and (3.20), the integral can be evaluated in closed from with the result

$$E_{\mathrm{APB}}=\tfrac{4}{3}(1+\alpha)|F_0|d_{\mathrm{APB}} , \tag{3.25}$$

where

$$\alpha=-[c_{12}B_1-c_{11}B_2]\left[\frac{\hat{B}_{11}}{\hat{c}_{11}}-\frac{\hat{B}_{22}}{\hat{c}_{22}}\right]\Big/3A'c_{11} . \tag{3.26}$$

By setting $\alpha=0, A'\rightarrow A$ in Eqs. (2.25) and (3.25), and $K^{+}\rightarrow K$ in Eq. (3.19) one obtains the result for the simple kink solution for the OP without coupling to the strain.

IV. TWIN BOUNDARY

Twin boundaries in the tetragonal perovskite phase separate regions with different directions of the tetragonal-rotational axis and consist of {110} planes.[15] We consider a $(1\bar{1}0)$ TB which separates the two regions with OP's $\mathbf{Q}=(Q_1,0,0)$ and $\mathbf{Q}=(0,Q_2,0)$. It is convenient to introduce the coordinate system

$$\begin{bmatrix} r \\ s \end{bmatrix}=\mathbf{E}\begin{bmatrix} x_1 \\ x_2 \end{bmatrix} , \tag{4.1a}$$

$$\mathbf{E}=\begin{bmatrix} \frac{1}{\sqrt{2}} & \frac{1}{\sqrt{2}} \\ -\frac{1}{\sqrt{2}} & \frac{1}{\sqrt{2}} \end{bmatrix} , \tag{4.1b}$$

where $\mathbf{E}$ represents a rotation by 45° around x_3, and s is in the direction of the TB normal [Fig. 4(a)]. Proceeding along similar lines as for the APB, the continuous TB profile is described by the two-component OP

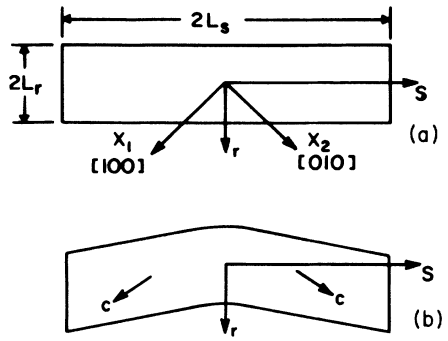

FIG. 4. (a) Dimensions and orientation of (001) section of rectangular crystal bar in cubic parent phase with respect to two coordinate systems. (b) (001) section of bicrystal with continuous (110) twin boundary at $s=0$, obtained by ferroelastic transformation of crystal bar as in (*a*) into two variants of tetragonal product phase. The direction of the tetragonal *c* axis is for $c/a>1$ indicated by arrows (schematic).

$$Q=(Q_1,Q_2,0)\ , \tag{4.2a}$$

and we seek solutions where Q_1,Q_2 depend on the variable s only, but not on r and x_3:

$$Q_1=Q_1(s),\ Q_2=Q_2(s)\ . \tag{4.2b}$$

Then the coupling between Q and the strain and stress implies that

$$\eta_{ij}=\eta_{ij}(s)\ , \tag{4.3a}$$

$$\sigma_{ij}^{\rm tot}=\sigma_{ij}^{\rm tot}(s)\ . \tag{4.3b}$$

Consider now an infinitely long rectangular bar-shaped crystal specimen in the cubic state with dimensions $2L_r$, $2L_s\to\infty$ and $2L_3$ along the directions r, s, and x_3, respectively [Fig. 4(a)] that transforms into a twinned bicrystal, consisting of two regions with the tetragonal-rotational axis along x_1 for $s\to-\infty$, and along x_2 for $s\to+\infty$, that are separated by a $(\bar{1}10)$ TB at $s=0$ (Fig. 4b). Then for stress-free boundaries at $s\to\pm\infty$,

$$\lim_{s\to\pm\infty}\sigma_{ij}^{\rm tot}(s)=0\ , \tag{4.4}$$

at $s\to\pm\infty$ the crystal is in the two homogeneous single domain tetragonal states that are described in terms of the boundary conditions for the OP and for the strain, both referred to the x_1,x_2, and x_3 axes, as given in Table II. The corresponding boundary conditions for the OP and for the strain, referred to the rotated coordinate system, become

$$\lim_{s\to\pm\infty}Q_r=Q_0/\sqrt{2}\ , \tag{4.5a}$$

$$\lim_{s\to\pm\infty}Q_s=\pm Q_0/\sqrt{2}\ , \tag{4.5b}$$

$$\lim_{s\to\pm\infty}\eta_{rr}=\lim_{s\to\pm\infty}\eta_{ss}=(\eta_{\parallel}+\eta_{\perp})/2\ , \tag{4.6a}$$

$$\lim_{s\to\pm\infty}\eta_{rs}=\pm(\eta_{\parallel}-\eta_{\perp})/2\ . \tag{4.6b}$$

TABLE II. Boundary conditions for OP and strain, both referred to the x_1,x_2,x_3 coordinate system, of a tetragonal bicrystal with a (110) TB at $s=0$, as shown in Fig. 4. Q_0, $\eta_{\parallel}$, and $\eta_{\perp}$ are defined by Eqs. (2.24), (2.26a), and (2.26b), respectively.

s	$-\infty$	$+\infty$
Q	$(Q_0,0,0)$	$(0,Q_0,0)$
η	$\begin{bmatrix}\eta_{\parallel}&&\\&\eta_{\perp}&\\&&\eta_{\perp}\end{bmatrix}$	$\begin{bmatrix}\eta_{\perp}&&\\&\eta_{\parallel}&\\&&\eta_{\perp}\end{bmatrix}$

In addition to Eq. (4.4) we prescribe the boundary conditions

$$\sigma_{s3}(s)=\sigma_{r3}(s)\equiv 0\ . \tag{4.7}$$

With the ansatz given by Eqs. (4.2) and (4.3) the total LGFE [Eq. (2.1)] becomes

$$F=F_L(Q_r,Q_s)+F_G(Q_{r,s},Q_{s,s})+F_{\rm el}(\eta_{kl})+F_c(Q_r,Q_s,\eta_{kl})\ , \tag{4.8}$$

where

$$F_L=\frac{K}{2}(Q_r^2+Q_s^2)+A(Q_r^2+Q_s^2)^2+\frac{A_n}{4}(Q_r^2-Q_s^2)^2\ , \tag{4.9}$$

$$F_G=\frac{D_{rs}}{2}Q_{r,s}^2+\frac{D_{ss}}{2}Q_{s,s}^2\ , \tag{4.10}$$

and

$$D_{rs}=[D_{11}-D_1]/2\ , \tag{4.11a}$$

$$D_{ss}=[D_{11}+D_{12}+2D_{44}]/2\ . \tag{4.11b}$$

$F_{\rm el}$ and F_c are given by Eqs. (2.9) and (2.10), with e_α and P_α expressed in terms of the quantities in the new coordinate system as follows:

$$\begin{bmatrix}P_1\\P_3\\P_6\end{bmatrix}=\mathbf{T}\begin{bmatrix}Q_r^2\\Q_s^2\\0\end{bmatrix}\ , \tag{4.12a}$$

$$P_2=-\sqrt{2}Q_rQ_s\ , \tag{4.12b}$$

$$P_4=P_5=0\ , \tag{4.12c}$$

$$\begin{bmatrix}e_1\\e_3\\e_6\end{bmatrix}=\mathbf{T}\begin{bmatrix}\eta_{rr}\\\eta_{ss}\\\eta_{33}\end{bmatrix}\ , \tag{4.13a}$$

$$e_2=-\sqrt{2}\eta_{rs}\ , \tag{4.13b}$$

$$e_4=\sqrt{2}(\eta_{r3}+\eta_{s3})\ , \tag{4.13c}$$

$$e_5=\sqrt{2}(\eta_{r3}-\eta_{s3})\ , \tag{4.13d}$$

where

$$\mathbf{T}=\begin{bmatrix} \frac{1}{\sqrt{3}} & \frac{1}{\sqrt{3}} & \frac{1}{\sqrt{3}} \\ \frac{1}{\sqrt{6}} & \frac{1}{\sqrt{6}} & -\frac{2}{\sqrt{6}} \\ 1 & -1 & 0 \end{bmatrix} . \tag{4.14}$$

Then the components of the total stress tensor become

$$\sigma_{ij}^{\text{tot}}=\sum_{\alpha=1}^{6} H_{ij\alpha}\{\hat{c}_{\alpha\alpha}e_\alpha-\hat{B}_{\alpha\alpha}P_\alpha\} \quad (i,j=r,s,3) , \tag{4.15}$$

where $H_{ij\alpha}=(\partial e_\alpha/\partial\eta_{ij})$ are numerical coefficients[43] that are determined by Eqs. (4.13) and (4.14). It now follows immediately from Eqs. (4.7) and (4.15) that

$$\eta_{r3}=\eta_{s3}\equiv 0 . \tag{4.16}$$

In view of Eq. (4.3a) the compatibility relations [Eqs. (3.10)] reduce to

$$\eta_{rr,ss}=0 , \tag{4.17a}$$

$$\eta_{33,ss}=0 , \tag{4.17b}$$

$$\eta_{r3,ss}=0 . \tag{4.17c}$$

Whereas in view of Eq. (4.16) Eq. (4.17c) is trivially satisfied, integration of Eqs. (4.17a) and (4.17b) gives, in conjunction with Eq. (4.6a) and Table II, respectively,

$$\eta_{rr}=\tfrac{1}{2}(\eta_{\parallel}+\eta_{\perp}) , \tag{4.18a}$$

$$\eta_{33}=\eta_{\perp} . \tag{4.18b}$$

Since the constancy of η_{rr} and η_{33}, as expressed in Eqs. (4.18a) and (4.18b), is a consequence of the compatibility relations in conjunction with the ansatz of Eq. (4.2), it is apparent that in order to sustain the quasi-1D solution according to Eqs. (4.2) and (4.3) without interface dislocations and/or disclinations the crystal must be laterally constrained ("clamped") in the r and x_3 directions.

In view of Eq. (4.3b) the equilibrium conditions (2.15) reduce to

$$\sigma_{rs,s}^{\text{tot}}=\sigma_{ss,s}^{\text{tot}}=\sigma_{3s,s}^{\text{tot}}=0 . \tag{4.19}$$

In conjunction with the boundary conditions (4.4), it follows immediately that

$$\sigma_{rs}^{\text{tot}}=0 , \tag{4.20a}$$

$$\sigma_{ss}^{\text{tot}}=0 , \tag{4.20b}$$

$$\sigma_{3s}^{\text{tot}}=0 . \tag{4.20c}$$

Equations (4.15) and (4.20c) simply recover the result $\eta_{s3}=0$ from Eq. (4.16). The remaining two strain components, η_{rs} and η_{ss}, depend on position and may be obtained from Eqs. (4.15), (4.20a), and (4.20b) in the form

$$\eta_{rs}=[(B_1-B_2)/(c_{11}-c_{12})]Q_rQ_s , \tag{4.21a}$$

$$\eta_{ss}=\eta_{ss}^{\infty}-[(B_1+B_2)G(s)+B_tH(s)]/(2c_{rr}) , \tag{4.21b}$$

where

$$G(s)=Q_0^2-(Q_r^2+Q_s^2) , \tag{4.22a}$$

$$H(s)=Q_r^2-Q_s^2 , \tag{4.22b}$$

and

$$c_{rr}=c_{ss}=(c_{11}+c_{12})/2+c_{44} . \tag{4.23}$$

From the boundary conditions (4.5) it is apparent that

$$\lim_{s\to\pm\infty} G(s)=\lim_{s\to\pm\infty} H(s)=0 . \tag{4.24}$$

η_{ss}^{∞} is given by Eq. (4.6b).

According to Eqs. (4.7) and (4.19), four stress components vanish identically. The remaining nonzero components are obtained by inserting the strains from Eqs. (4.16), (4.18), and (4.21) into Eq. (4.15) with the result

$$\sigma_{rr}^{\text{tot}}=\frac{1}{2c_{rr}}[2c_{44}(B_1+B_2)G(s) -(c_{11}+c_{12})B_tH(s)] , \tag{4.25a}$$

$$\sigma_{33}^{\text{tot}}=\frac{1}{2c_{rr}}\{[-c_{12}B_1+(c_{11}+2c_{44})B_2]G(s) -c_{12}B_tH(s)\} . \tag{4.25b}$$

These are the position dependent stresses required to clamp the crystal laterally so as to sustain the quasi-1D solutions postulated in (4.2) and (4.3).

The equilibrium conditions (2.14) for the OP become explicit after expressing the strains in terms of Q_r and Q_s

$$D_{rs}Q_{r,ss}=K_rQ_r+4A_rQ_r^3+4A_{rs}Q_rQ_s^2 , \tag{4.26a}$$

$$D_{ss}Q_{s,ss}=K_sQ_s+4A_sQ_s^3+4A_{rs}Q_sQ_r^2 , \tag{4.26b}$$

where

$$K_r=K\left[1+\frac{1}{4A'}\left[\frac{2\hat{B}_{11}^2}{3\hat{c}_{11}}+\frac{\hat{B}_{33}^2}{3\hat{c}_{33}} -\frac{(B_1+B_2)(B_1+B_2-B_t)}{2c_{ss}}\right]\right] , \tag{4.27a}$$

$$K_s=K\left[1+\frac{1}{4A'}\left[\frac{2\hat{B}_{11}^2}{3\hat{c}_{11}}+\frac{\hat{B}_{33}^2}{3\hat{c}_{33}} -\frac{(B_1+B_2)(B_1+B_2+B_t)}{2c_{ss}}\right]\right] , \tag{4.27b}$$

$$A_r=A+\frac{A_n}{4}-\frac{(B_1+B_2-B_t)^2}{8c_{ss}} , \tag{4.27c}$$

$$A_s=A+\frac{A_n}{4}-\frac{(B_1+B_2+B_t)^2}{8c_{ss}} , \tag{4.27d}$$

$$A_{rs}=A-\frac{A_n}{4}-\frac{1}{4}\left[\frac{(B_1+B_2)^2-B_t^2}{2c_{ss}}+\frac{2\hat{B}_{33}^2}{\hat{c}_{33}}\right] . \tag{4.27e}$$

Equations (4.26) depend on seven material parameters and must, in general, be solved numerically. However, for vanishing coupling parameter

$$A_{rs}=0 \tag{4.28}$$

the following interrelations exist:

$$K_r/A_r=K_s/A_s=K/(2A') , \tag{4.29}$$

and *for the preceding boundary conditions* Eqs. (4.26) have the analytic solution

$$Q_r=Q_0/\sqrt{2} , \tag{4.30a}$$

$$Q_s=(Q_0/\sqrt{2})\tanh(s/\xi^0_{\mathrm{TB}}) , \tag{4.30b}$$

where

$$\xi^0_{\mathrm{TB}}=d^0_{\mathrm{TB}}/2=\sqrt{-2D_{ss}/K_s} \tag{4.31}$$

is half the twin boundary thickness d^0_{TB} and the superscript 0 refers to the condition $A_{rs}=0$. The OP components Q_1 and Q_2 are given by the kink-type solutions

$$\begin{aligned} Q_1&=(Q_0/2)[1-\tanh(s/\xi_{\mathrm{TB}})] ,\\ Q_2&=(Q_0/2)[1+\tanh(s/\xi_{\mathrm{TB}})] \end{aligned} \tag{4.32}$$

and describe a continuous transition between the two homogeneous states of $s=\pm\infty$ (Table II). The associated position-dependent strain components become

$$\eta_{rs}=(\hat{B}_{33}/2\hat{c}_{33})Q_0^2\tanh(s/\xi_{\mathrm{TB}}) , \tag{4.33a}$$

$$\eta_{ss}=\eta_{ss}^{\infty}-(Q_0^2/4c_{rr})(B_1+B_2+B_t)\operatorname{sech}^2(s/\xi_{\mathrm{TB}}) . \tag{4.33b}$$

Equation (4.33a) describes the shape change of the bicrystal that results from the presence of the twin boundary as illustrated schematically in Fig. 4(b). Equation (4.33b) describes the longitudinal strain in the direction of the TB normal; the first term represents a contraction-dilation and arises from the O_h-D_{4h} transformation even in the absence of the TB; the second term represents a longitudinal length change by the amount

$$\Delta L_s=-(Q_0^2/2c_{rr})(B_1+B_2+B_t)\xi_{\mathrm{TB}}$$

that is due to the TB [Fig. 4(b)]. The associated nonvanishing components of the stress tensor become

$$\sigma^{\mathrm{tot}}_{rr}=(Q_0^2/4c_{rr})[2c_{44}(B_1+B_2)-(c_{11}+c_{12})B_t]\operatorname{sech}^2(s/\xi_{\mathrm{TB}}) , \tag{4.34a}$$

$$\sigma^{\mathrm{tot}}_{33}=(Q_0^2/4c_{rr})[-c_{12}(B_1+B_t)+(c_{11}+2c_{44})B_2]\operatorname{sech}^2(s/\xi_{\mathrm{TB}}) . \tag{4.34b}$$

For the special case corresponding to Eq. (4.28) the energy density of a single TB defined in analogy to Eq. (3.24) can be evaluated in closed from with the result

$$E_{\mathrm{TB}}=\tfrac{2}{3}(1+\delta)|F_0|d^0_{\mathrm{TB}} , \tag{4.35}$$

where

$$\delta=\frac{1}{4A'}\left[\frac{2\hat{B}^2_{11}}{3\hat{c}_{11}}+\frac{\hat{B}^2_{33}}{\hat{c}_{33}}-\frac{(B_1+B_2)(B_1+B_2+B_t)}{2c_{rr}}\right] . \tag{4.36}$$

For treating the general case $A_{rs}\neq 0$ it is convenient to introduce dimensionless variables according to

$$Q_r=(Q_0/\sqrt{2})q_r , \tag{4.37a}$$

$$Q_s=(Q_0/\sqrt{2})q_s \tag{4.37b}$$

$$s=\gamma z , \tag{4.37c}$$

where

$$\gamma=[D_{rs}D_{ss}/K_rK_s]^{1/4} \tag{4.38}$$

is a characteristic length. Then the boundary conditions (4.5a) and (4.5b) and the equilibrium conditions (4.26) become, in terms of the dimensionless OP, respectively,

$$\lim_{z\to\pm\infty} q_r=1 , \tag{4.39a}$$

$$\lim_{z\to\pm\infty} q_s=\pm 1 , \tag{4.39b}$$

and

$$\frac{1}{a}q_r''+q_r-(1-\alpha_r)q_r^3-\alpha_r q_r q_s^2 , \tag{4.40a}$$

$$aq_s''+q_s-(1-\alpha_s)q_s^3-\alpha_s q_r^2 q_s . \tag{4.40b}$$

Here the prime denotes differentiation with respect to z, and three dimensionless parameters have been defined as

$$a=[D_{ss}K_r/D_{rs}K_s]^{1/2} , \tag{4.41a}$$

$$\alpha_r=A_{rs}/(A_r+A_{rs}) , \tag{4.41b}$$

$$\alpha_s=A_{rs}/(A_s+A_{rs}) \tag{4.41c}$$

In deriving Eqs. (4.40a) and (4.40b) use has been made of the relations

$$K_r/(A_r+A_{rs})=K_s/(A_s+A_{rs})=K/(2A')=-2Q_0^2 . \tag{4.42}$$

The Eqs. (4.40a) and (4.40b) have the first integral

$$\alpha_r\alpha_s^2(q_r')^2+a^2\alpha_r^2\alpha_s(q_s')^2+a\alpha_r\alpha_s^2(q_r^2-1)+a\alpha_r^2\alpha_s(q_s^2-1)-\tfrac{1}{2}a\alpha_r(1-\alpha_r)\alpha_s^2(q_r^4-1)-(\tfrac{1}{2})a\alpha_r^2\alpha_s(1-\alpha_s)(q_s^4-1)-a\alpha_r^2\alpha_s^2(q_r^2q_s^2-1)=0 \tag{4.43}$$

With the aid of Eq. (4.43) the equilibrium conditions may be integrated by means of a nonlinear initial value scan method.[44] Figure 5 shows examples of OP profiles for various parameter values a and α_r obtained in this manner under the assumption $\alpha_r=\alpha_s$. The range of parameter values chosen includes those pertaining to $SrTiO_3$ to be discussed in Sec. V. The curves for q_r and q_s shown for the parameter values $\alpha_r=\alpha_s=0$ are independent of the parameter a and represent the analytic solution given by Eq. (4.30).

It is apparent that for the range of parameter values covered in Fig. 5 the salient feature of the TB profile is the kink, described by the q_s, and that the hump (or dip), described by q_r, plays a secondary role. The hump is characterized by its relative magnitude $|q_r-1|_{\max}$ and its half width. The kink width $d_{\rm TB}$ is defined by

$$q_s(z)|_{z=d_{\rm TB}/2\gamma}=\tanh 1=0.7617\ , \tag{4.44}$$

which reduces for $\alpha_r=\alpha_s=0$ to the intrinsic value $d^0_{\rm TB}=2\xi^0_s$ given by Eq. (4.31). Both the height of the hump $|q_r-1|_{\max}$ and the kink width $d_{\rm TB}$ increase with increasing values of $\alpha_r=\alpha_s$ and a, but the hump is more affected by the coupling constant $\alpha_r=\alpha_s$, and the kink by the parameter a.

It is worth noting that the parameter γ is essentially the geometric mean of the two intrinsic length scales of q_r and q_s, respectively, viz.,

$$\gamma=(\xi^0_r\xi^0_s/2)^{1/2}\ , \tag{4.45}$$

where in analogy to Eq. (4.31)

$$\xi^0_r=(-2D_{rs}/K_s)^{1/2} \tag{4.46}$$

and, furthermore,

$$a=\xi^0_s/\xi^0_r\ . \tag{4.47}$$

It should further be noted that the three parameters entering Eqs. (4.40a) and (4.40b), and therefore the results in Fig. 5, are independent of temperature when, as usual, the temperature enters the LGFE [Eq. (2.1)] only through the soft-mode harmonic force constant $K=K(T)$. In this case [because of Eqs. (4.27a), (4.27b), and (4.29)] the temperature dependence of the TB profile arises only from the temperature dependence of the characteristic length γ according to

$$\gamma(T)=[K(T_0)/K(T)]^{1/2}\gamma(T_0)\ . \tag{4.48}$$

Therefore, the temperature dependence of the TB thickness, in view of Eq. (4.44), is given by

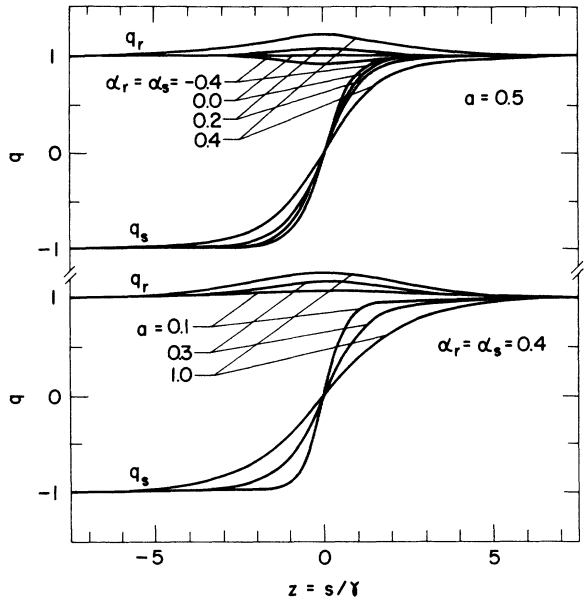

FIG. 5. Order-parameter profile from Eqs. (4.40a) and (4.40b) for selected values of input parameters.

$$d_{\rm TB}(T)=[K(T_0)/K(T)]^{1/2}d_{\rm TB}(T_0)\ . \tag{4.49}$$

In the general case of nonvanishing coupling constants the TB energy must be evaluated by numerical integration. However, since for the range of parameter values covered in Fig. 5 the height of the hump $|q_r-1|_{\max}\leq 0.25$, one may neglect the contribution from q_r, and then use Eq. (4.35) but with the TB width pertaining to the actual parameter values a,α_r,α_s as determined from Eq. (4.44). This is tantamount to approximating the different kink profiles in Fig. 5 using the uncoupled solutions $q_s=\tanh s/\gamma$ with the same initial slope at $s=0$ as the actual solutions $q_s(s/\gamma)$. Therefore, in view of Eq. (4.49) the temperature dependence of the TB energy is approximately given by

$$E_{\rm TB}=[K(T_0)/K(T)]^{3/2}E_{\rm TB}(T_0)\ . \tag{4.50}$$

V. APPLICATION TO $SrTiO_3$

$SrTiO_3$ is the only perovskite for which *all* experimental input data required for the numerical application of the preceding theory are available. In Table III these data (except for the elastic constants) plus an average value of the soft-mode force constant K from Fig. 4 of Slonczewski and Thomas[10] are listed for the reference

TABLE III. Experimental input data for $SrTiO_3$ at 78 K. Q_0 denotes a component of the primary order parameter, $\sigma_s=(c/a)-1=\eta_\parallel-\eta_\perp$ denotes spontaneous strain, ω_1,ω_3 are soft-mode frequencies in the tetragonal phase, $M=2M_0/a^3$ denotes effective mass density of oxygen ions, and K denotes harmonic expansion coefficient of order parameter. References are given in parentheses.

Q_0 (7)	σ_s (45)	ω_1 (1)	ω_3 (1)	M	K/M (10)
(nm)	(10^{-4})	($10^{12}\sec^{-1}$)	($10^{12}\sec^{-1}$)	($10^3\,\mathrm{kg\,m^{-3}}$)	($10^{24}\sec^{-2}$)
0.0047	4.0	2.167	6.593	0.898	−15.45

temperature $T_0=78$ K. Table IV contains the remaining (in addition to K) expansion coefficients of the Landau-Ginzburg free energy, Eqs. (2.1) to (2.5). $\kappa_{\mu\nu}$ and $B_{\mu\nu}$ were calculated from the data of Table III in the same manner as in Ref. 10. Specifically, the small volume change associated with the O_h-D_{4h} transition[47–49] was neglected, so that $B_1+2B_2=0$. The elastic constants $c_{\mu\nu}$ were extrapolated linearly from experimental data[46] in the high-temperature regime of the cubic phase so as to eliminate the contributions from fluctuations of the primary order parameter.[50,51] The rotation gradient coefficients $D_{\mu\nu}$ were calculated by means of the procedure outlined in the Appendix from experimental phonon dispersion data[52] of the soft mode in the vicinity of the R point.

Figures 6(a) and 6(b) show a schematic representation of the displacement pattern of the oxygen ions across the TB and the OP profile $Q_1(s)$,$Q_2(s)$ in physical units, respectively. The latter was obtained by numerical integration of Eqs. (4.40a) and (4.40b) with the parameter values [cf. Eqs. (4.41a), (4.41b), and (4.41c)]

$$a=0.983,\ b=0.433,\ c=0.440$$

as calculated from the data of Table IV. The curves for the quantities $q_r(s)$, $q_s(s)$ pertaining to the dimensionless variables in the rotated coordinate system (r,s,x_3) are approximately equal to the set for $a=1$, $\alpha_r=\alpha_s=0.4$ in Fig. 5.

In Figs. 7(a) and 7(b) the induced-strain components η_{ij} [$ij=11$, 22, 33, 12 and $ij=rr,ss,rs$; see Fig. 3] and the surface-stress components $\sigma_{rr}^{\rm tot}$ and $\sigma_{33}^{\rm tot}$ required to sustain the quasi-1D OP profile of Fig. 6(b) are shown versus position. It is apparent that at the TB center [$s=0$] the crystal symmetry is *approximately* tetragonal, but with the tetragonal axis being contracted along the x_3 axis. However, there is a small monoclinic deformation present at the center. The maximum stress $\sigma_{33}^{\rm tot}=4.76\times10^7$ Nm^{-2} is smaller than the yield stress [about 10^{-3} times the appropriate shear modulus], so that no plastic deformation in the TB should occur. However, for a bicrystal with free boundaries the twin boundary would bulge out both in the r and the 3 direction and the solutions for the primary OP and for the strain would depend on all three spatial variables.

Finally, Fig. 8 shows the widths $d_{\rm APB}$ and $d_{\rm TB}$, and the energy densities $E_{\rm APS}$ and $E_{\rm TB}$ for the APB's and for the TB's versus temperature as calculated from the mean of

TABLE IV. Expansion coefficients of Landau-Ginzburg free energy [Eqs. (2.1)–(2.5)] for $SrTiO_3$ in Voigt notation. It is $\kappa_{11}=2A$, $\kappa_{12}=2A+A_n$; $B_{11}=B_1$, $B_{12}=B_2$, $B_{44}=B_t$.

$\mu\nu$	11	12	44	Ref.
$\kappa_{\mu\nu}$ (10^{50} N m^{-6})	3.63	3.82		10
$c_{\mu\nu}$ (10^{11} N m^{-2})	3.365	1.047	1.269	46
$B_{\mu\nu}$ (10^{30} N m^{-4})	2.80	−1.40	2.54	10
$D_{\mu\nu}$ (10^{9} N m^{-2})	0.07	−1.86	1.80	28

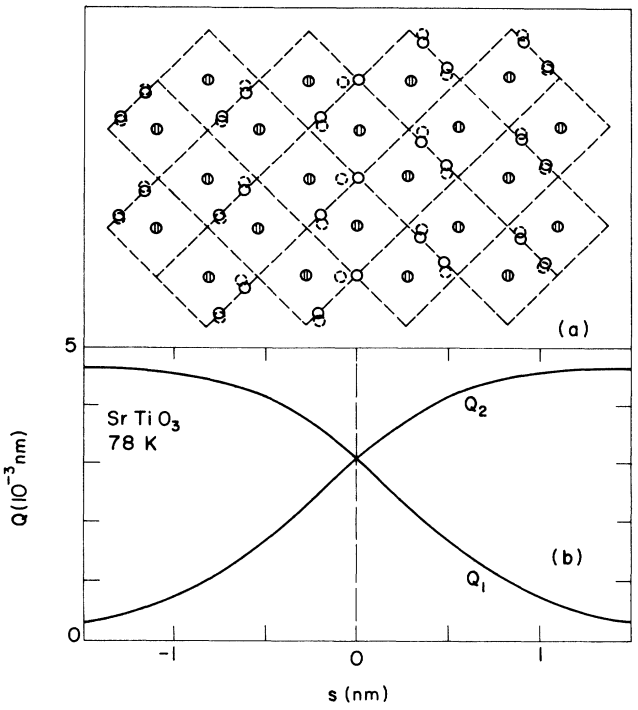

FIG. 6. (a) Displacement pattern of X ions in vicinity of twin boundary at $s=0$ (schematic). The open circle is a discontinuous twin boundary; the dashed circle is a continuous order parameter profile according to this model. Shape change due to induced elastic transformation strain is not shown. (b) Order-parameter profile in physical units for $SrTiO_3$ at 78 K.

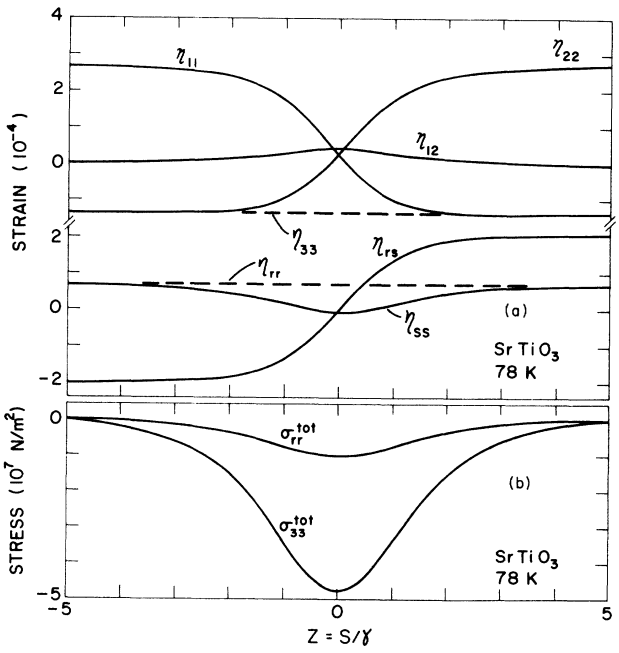

FIG. 7. Position dependence of strain and surface stress components across twin boundary for $SrTiO_3$ at 78 K. (a) Strain profile. (b) Surface stresses.

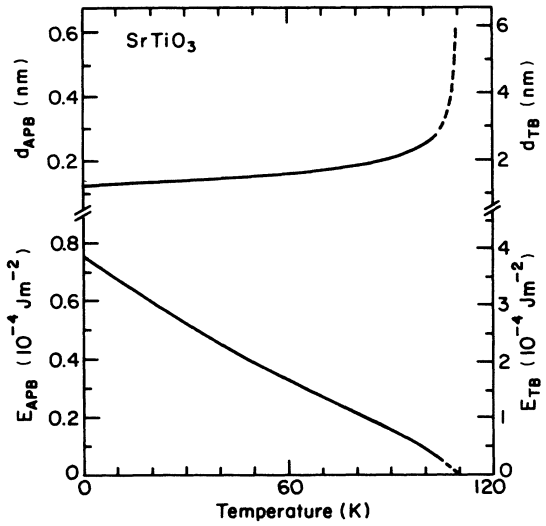

FIG. 8. Energy E and width d of antiphase boundary (APB) and twin boundary (TB), respectively, vs temperature for $SrTiO_3$.

the empirically determined nonlinear temperature variation $K(T)$ of Slonczewski and Thomas [Fig. 4 of Ref. 10] according to Eqs. (3.19), (4.49), (3.25), and (4.50), respectively. Above 105 K the curves are given in dashed form to indicate the uncertainty associated with the present results based on mean-field theory as the critical point is approached. As usual for APB's, the APB for $SrTiO_3$ is atomically sharp at practically all temperatures: the calculated width is 0.32 a_0 [a_0 denotes the lattice parameter which is 3.90 Å] at absolute zero and increases to about $1.03a_0$ at $(T_c-2)K=106$ K. The calculated width of the TB is 3.1 a_0 at $T=0$, 4.9 a_0 at $T=90$ K, and about 10 a_0 at 106 K. Although ferroelastic domains have been observed in $SrTiO_3$ by optical microscopy,[12] no measurements of d_{TB} are available. However, the *ferroelectric* TB's in KDP have been studied by x-ray diffraction[18] and found to behave semiquantitatively very similar to the calculated results of Fig. 8: the measured values of d_{TB} [as defined here] are 4.2 a_0, 7.4 a_0 and 9.7 a_0 at $T=0,90$ K, and $T_c-2=119.4$ K, respectively.[18]

According to Fig. 8, the energy of the APB (TB) decreases approximately linearly with temperature from 0.075 erg cm^{-2} [0.38 erg cm^{-2}] at absolute zero, to zero a T_c. The approximately linear temperature dependence arises from the nonlinear temperature dependence of $K(T)$ determined by Slonczewski and Thomas[10] in conjunction with the dependence $E_{TB}\sim K^{-3/2}$ [Eq. (4.50)]. For the APB's 4%, and for the TB's 5% of the interface energy arises from the coupling between the OP and the strain.

For comparison, the TB energy for $In_{0.79}Tl_{0.21}$ at 206 K, which undergoes a *proper* O_h-D_{4h} ferroelastic transition at 326 K, has been calculated from a Landau-Ginzburg model[53] as 1.1 erg cm^{-2}. Theoretical estimates for the energy of ferroelectric domain-wall energies in $BaTiO_3$ (at 300 K) are 2–4 erg cm^{-2} and 3.5 erg cm^{-2} [Refs. 20 and 21, respectively] for 90° walls, and about[20,21] 10 erg cm^{-2} for 180° walls.

VI. DISCUSSION

A. Significance and motivation

This work was envisioned as a rigorous treatment of a physically plausible and realistic model for interfaces in ferroic materials and constitutes a first step toward the study of the static and dynamic properties of interfaces in improper ferroelastics and their effect on physical properties, which show well known but not fully understood anomalous behavior near the transition temperature. The O_h-D_{4h} improper ferroelastic transition in perovskites was chosen because of all ternary compounds with composition ABX_3 the perovskites "are probably the most numerous, the most widely studied, and the most important" (Ref. 54). Specifically, since $SrTiO_3$ is probably the most thoroughly studied improper ferroelastic, all empirical input parameters are known, and numerical application of the theory was possible. In fact, we believe that this work and numerical results represent the first *consistent and complete* theoretical treatment (within the framework of the chosen model and with empirical input parameters) of interfaces in a ferroic material.

Because the symmetry properties of the zone corner R_{25} mode in perovskites are identical with those of the ferroelectric zone-center Γ_{15} mode[55] the LGFE, Eqs. (2.1) to (2.5) is formally very similar to that used in the early work on proper ferroelectric–improper ferroelastics,[20,21] except that the rotational invariance and the anisotropy of the (in that work, polarization) gradient terms were not taken into account, and the numerical values used for the gradient terms were not based on empirically input data. We will show in a forthcoming paper[56] how our results can be carried over with minor modifications to *ferroelectric* domain walls in perovskites.

B. Effect of coupling between order parameter and strain

Coupling between the OP and strain was already included in the early work on proper ferroelectric domain walls in perovskites and shown to result in a quasi-1D strain profile.[20,21] More recently, Lajzerowicz[57] considered a Landau-Ginzburg model for domain walls in an elastically isotropic uniaxial proper ferroelectric undergoing a first-order phase transition with electrostrictive coupling between the (scalar) order parameter and strain included. For elastic isotropy (c_{11}-$c_{12}=2c_{44}$) and with $B_2=B_t=0$ the preceding kink solution [Eq. (3.18)] and the energy [Eq. (3.25)] for the APB become identical with Lajzerowicz's result if the coefficient of the sixth-order term in his Ginzburg-Landau free energy is set equal to zero.

The main objective of Ref. 57 was to show that for a first-order transition without electrostrictive coupling the width of the domain wall diverges at the transition temperature, but that by including this coupling the transition temperature in the domain wall is changed and "the domain wall does not diverge being clamped by the elastic coupling with the bulk" [Ref. 57]. We consider the wording of this conclusion to be misleading, because the transition temperature is not changed "by the elastic cou-

pling with the bulk" (Ref. 57) but because the domain wall must be laterally stressed by surface forces that are required to sustain a quasi 1D solution.

Since the LGFE as given in Eqs. (2.1) to (2.5) describes a second-order phase transition the coupling between OP and strain does not affect the transition temperature in interphase boundaries. As is well known in mean-field theory, their width diverges, consistent within experimental resolution with measurements for the proper *ferroelectric* KDP.[18]

Finally, it should be noted that although for $SrTiO_3$ the surface stress required to sustain quasi-1D solutions and its contribution to the domain-wall energy are small and therefore seemingly of little practical significance, it is, of course, crucially important for the linear stability analysis and for future calculations of the vibrational excitation spectrum and its influence on all thermal properties.

C. Antiphase boundary lattice and twin band

The solutions for APB's and TB's already obtained describe individual interfaces and are defined by the boundary conditions, Eqs. (3.5), (3.6), and (4.4)–(4.7) over the *infinite* interval $(-\infty,\infty)$ for x_3 or s, respectively. For finite specimen length at the longitudinal faces ($x_3=\pm L_3$ or $s=\pm L_s$) the OP does not reach its extremal value $\pm Q_0$, as in Eqs. (3.5) and (4.5), corresponding to the minimum of the Landau free energy for the homogeneous phase, Eq. (2.20), but assumes a values $Q^*<Q_0$. This value is determined by L_3 or L_s, and by the number of kinks and antikinks in the interval $(-L_3,L_3)$ or $(-L_s,L_s)$, respectively. In this case the stress components do not any longer all vanish at the lateral surfaces. The solutions for the APB lattice and, for the special case $A_{rs}=0$, for the twin band are periodic and are given by the Jacobi elliptic function[58,59] $sn(x,k)$, with the modulus k determined by Q^*.

D. Limitations of theory

It goes without saying that the numerous approximations underlying our model, while resulting in conceptual and mathematical simplicity, are also responsible for its limitations. First, the model is phenomenological and requires no less than 13 empirical parameters, viz., the 12 expansion coefficients of the LGFE, Eqs. (2.1)–(2.5), plus the temperature coefficient of the harmonic soft-mode force constant K. Reduction of the truncation errors implied in this expansion would further increase the number of parameters. Second, its continuum theoretical nature limits applicability to interface widths large compared to the lattice spacing a. In practice, this means[60] $d\geq 3a$, so that for $SrTiO_3$ numerical application to TB's is justified, but that the calculated values for the width and energy of APB's are no more than estimates. Furthermore, some parameter values were determined by using equations of questionable validity,[10] and in the tetragonal phase the soft-mode force constant K, when calculated from experimental data within the framework of the Landau model of Slonczewski and Thomas[10] does not follow a linear temperature dependence.

Possibilities for alternative approaches and improvement of the theory include use of the semimicroscopic phenomenological model of Pytte and Feder[61] and inclusion of fluctuations beyond mean-field theory.[62]

VII. SUMMARY AND CONCLUSIONS

We have presented a continuum theoretical model for APB's and TB's in the tetragonal phase of perovskites that results from the zone corner (R_{25}) mode-driven *improper* FE phase transition from the cubic prototype phase. The LGFE has been truncated so as to retain nonlinear terms in the local, and nonlocal gradient terms in the harmonic approximation for the primary OP, plus elastic energy terms in the harmonic approximation and lowest-order anharmonic coupling terms between the primary OP and strain. Our aim was to obtain solutions for the primary OP and for the strain that depend only on the spatial coordinate normal to the interface plane and that describe the shape change associated with planar interfaces in ferroelastics. For APB's these solutions are given by the familiar ϕ^4-type kinks for the primary OP. For TB's, in general, numerical solution of two coupled nonlinear second-order ordinary differential equations for a two-component OP is necessary. In both cases, for a crystal that is free of dislocations and disclinations, lateral surface forces are required over the thickness of the interfaces in order to sustain the dependence on only one spatial variable. On the other hand, for stress-free surfaces lateral strains in the interface plane would occur; the solution of this fully 3D case remains as a future task.

Numerical application to $SrTiO_3$ indicates atomically sharp APB's with energy decreasing from 0.075 erg cm^{-2} at $T=0$ to zero at the transition temperature T_c. The calculated width of TB's in $SrTiO_3$ increases from three (at $T=0$) to ten lattice constants (at T_c-2 K), and their energy decreases from 0.35 erg cm^{-2} at $T=0$ to zero at T_c. For APB's (TB's) only about 4% (5%) of the interface energy is due to the contribution from the strain.

ACKNOWLEDGMENTS

This work was supported by the U.S. Department of Energy under Grant No. DE-FG-02-85ER45214.

APPENDIX: DETERMINATION OF ROTATIONAL GRADIENT COEFFICIENTS

Here we show how the rotational gradient coefficients D_{11}, D_{12}, and D_{44} in the LGFE, Eq. (2.1) can be determined from the dispersion of the phonon branches into which the soft R_{25} mode frequency splits along the principal symmetry directions in the vicinity of the R point.

Considering small amplitude oscillations of the octahedra, we obtain the equations of motion $\ddot{Q}_i=\delta F/\delta Q_i$ in the linearized form (no summation convention)

TABLE V. Parameter $W_\mu(\hat{\mathbf{q}})$ for different irreducible representations with $\mathbf{k}$ in the directions $R-\Gamma$, $R-X$, $R-M$.

$\hat{\mathbf{q}}$	μ	$W_\mu(\hat{\mathbf{q}})$
[111]	Λ_2	$(D_{11}+2D_{12}+4D_{44})/3$
[111]	Λ_3	$(D_{11}-D_{12}+D_{44})/3$
[110]	Σ_1	$(D_{11}-D_{12})/2$
[110]	Σ_2	D_{44}
[110]	Σ_4	$(D_{11}+D_{12}+2D_{44})/2$
[001]	Δ_2	D_{11}
[001]	Δ_5	D_{44}

TABLE VI. Comparison of experimental (Ref. 52) and calculated values of $\Lambda_\mu(\hat{\mathbf{q}})$ for $SrTiO_3$ at RT.

$\hat{\mathbf{q}}$	μ	Λ_μ (m^2/sec^2) Expt.	Calc.
[111]	Λ_3	131±23	138.7
[110]	Σ_1	112±22	107.31
[001]	Δ_5	205±27	201.5
[001]	Δ_2	8± 2	8

$$M\ddot{Q}_i - D_{11}Q_{i,jj} - D_{12}(Q_{j,ji}+Q_{k,ki}) - D_{44}(Q_{i,jj}+Q_{i,kk}+Q_{j,ij}+Q_{k,ik}) + KQ_i = 0 \ , (i,j,k,=1,2,3,\ i\neq j\neq k) \ . \tag{A1}$$

$M=2m_x/a^3$ is the effective mass density for the rotation of the BX_6 octahedra around any of the three cubic axes. Equation (A1) has plane-wave solutions

$$Q_i(\mathbf{x},t)=Q_i^0 e^{i(\mathbf{k}\cdot\mathbf{x}-\omega t)} \ . \tag{A2}$$

For $\mathbf{k}=\pi/a[1,1,1]=\mathbf{k}_R$, the octahedron at the lattice site $\mathbf{x}=a[l,m,n]$ oscillates according to

$$Q_i(\mathbf{x},t)=Q_i^0(-1)^{(l+m+n)}e^{-i\omega t} \ . \tag{A3}$$

Thus in the R_{25} mode, all neighboring octahedra rotate with the same amplitude, but in opposite directions. From Eqs. (A1) and (A3) one obtains the triply degenerate R_{25} mode frequency $\omega_R=(K/M)^{1/2}$ and eigenvectors $\langle 100\rangle$ that correspond to the rotation of the octahedra around one of the cubic axes. When $\mathbf{k}$ differs slightly from $\mathbf{k}_R$,

$$\mathbf{k}=\mathbf{k}_R-\mathbf{q}, \ |\mathbf{q}|\ll|\mathbf{k}_R| \ , \tag{A4}$$

Eq. (A2) becomes

$$Q_i(\mathbf{x},t)=Q_i^0(-1)^{(l+m+n)}e^{-i(\mathbf{q}\cdot\mathbf{x}+\omega t)} \ . \tag{A5}$$

First-order perturbation theory leads to the following eigenvalue problem:

$$\tilde{H}\mathbf{u}=M\omega^2\mathbf{u} \tag{A6}$$

with $\mathbf{Q}^0=Q^0\mathbf{u}$ and

$$\tilde{H}=\begin{bmatrix} K+D_{11}q_1^2+D_{44}(q_2^2+q_3^2) & (D_{12}+D_{44})q_1q_2 & (D_{12}+D_{44})q_1q_3 \\ (D_{12}+D_{44})q_1q_2 & K+D_{11}q_2^2+D_{44}(q_1^2+q_3^2) & (D_{12}+D_{44})q_2q_3 \\ (D_{12}+D_{44})q_1q_3 & (D_{12}+D_{44})q_2q_3 & K+D_{11}q_3^2+D_{44}(q_1^2+q_2^2) \end{bmatrix} \ . \tag{A7}$$

Except for a factor M, this matrix is identical with the truncated Taylor expansion of the 3×3 R_{25} block of the dynamical matrix of the perovskite structure with respect to $\mathbf{q}$ as given by Gesi *et al.*,[63] with their expansion coefficients related to those in Eq. (A7) according to $\lambda_1=D_{11}/M$, $\lambda_2=D_{44}/M$, and $\lambda_3=D_{12}+D_{44})/M$. These authors point out[63] that, because the group of the wave vector at the R point has O_h point-group symmetry, the matrix **H-KI** (**I** denotes the unit matrix) is formally identical with the Christoffel tensor, which has the eigenvalues $\rho\omega_\lambda^2$, where ω_λ ($\lambda=1,2,3$) are the long-wavelength acoustic mode frequencies in the direction $\hat{\mathbf{q}}$. Therefore, writing the eigenvalues of **H** in the form

$$M\omega_\mu^2(\mathbf{k})=K+W_\mu(\hat{\mathbf{q}})q^2 \tag{A8}$$

one obtains immediately the expansion coefficients $W_\mu(\hat{\mathbf{q}})$ along the three principal symmetry directions as given in Table V. There the branches μ are labeled according to the irreducible representations in the notation of Bouckaert *et al.*,[64] and the linear combinations of the rotational gradient coefficients are identical to those of the elastic constants in the corresponding eigenvalues of the Christoffel tensor.

For $SrTiO_3$ experimental phonon dispersion data for four different modes into which the R_{25} mode splits in the vicinity of the R point are available.[52] By means of least-squares fitting we have determined the three independent coefficients D_{11}, D_{12}, and D_{44} from these data and included the results in Table IV. In Table VI the experimental data[52] of $\Lambda_\mu(\hat{\mathbf{q}})$ as defined by Stirling[52] in the form

$$\omega_\mu^2(k)=\omega_{\mathbf{R}_{25}}^2+\Lambda_\mu(\hat{q})\mathbf{q}^2 \tag{A9}$$

are compared with those calculated from the fitted data in Table IV and the relations in Table V according to $\Lambda_\mu(\hat{\mathbf{q}})=W_\mu(\hat{\mathbf{q}})/M$. The agreement is well within the stated experimental error, indicating good internal consistency of the data. The consistency relation

$$3W_{\Lambda_3}=2W_{\Sigma_1}+W_{\Delta_5} \ , \tag{A10}$$

which follows from the Table V, is satisfied to within 9%.

In $SrTiO_3$ the O_h-D_{4h} transition occurs at about[8] 108 K. Although data below this temperature were also reported,[52] here we have considered only room-temperature data because the observed temperature dependence is small and because in the LG theory all expansion coefficients, except the harmonic one, are usually taken as temperature independent and are referred to the high-symmetry phase.

*Present address: Laboratory of Atomic and Solid State Physics, Cornell University, Ithaca, NY 14853-2501.

[1]P. A. Fleury, J. F. Scott, and J. M. Worlock, Phys. Rev. Lett. **21**, 16 (1968).

[2]A. Okazaki and Y. Suemune, J. Phys. Soc. Jpn. **16**, 671 (1961).

[3]F. Denoyer, R. Comès, M. Lambert, and A. Guinier, Acta Crystallogr. A **30**, 423 (1974).

[4]M. Rousseau, J. Nouet, and R. Almairac, J. Phys. (Paris) **38**, 1423 (1977).

[5]M. Rousseau, J. Y. Gesland, J. Julliard, J. Nouet, J. Zarembowitch, and Z. Zarembowitch, Phys. Rev. B **12**, 1579 (1975).

[6]J. C. Toledano and P. Toledano, Phys. Rev. B **21**, 1139 (1980).

[7]G. Shirane and Y. Yamada, Phys. Rev. **177**, 858 (1969).

[8]U. Unoki and T. Sakudo, J. Phys. Soc. Jpn. **23**, 546 (1967).

[9]H. Thomas and K. A. Müller, Phys. Rev. Lett. **21**, 1256 (1968).

[10]J. C. Slonczewski and H. Thomas, Phys. Rev. B **1**, 3599 (1970).

[11]u_i ($i=1,2,3$) denotes the components of the elastic displacement vector field $\mathbf{u}=\mathbf{u}(\mathbf{x})$, and indices $i,\ldots,$ preceded by a comma denote differentiation with respect to the component x_i of the position vector of a material point in the undeformed stress-free rerefence state. On the whole, in this paper we follow the notation of ST as closely as possible. However, we have introduced the factor $\frac{1}{2}$ in the definition of the strain tensor so that dilatational and shear strains are all components of *one* tensor.

[12]F. W. Lytle, J. Appl. Phys. **35**, 2212 (1964).

[13]C. Boulesteix, Phys. Status Solidi A **86**, 11 (1984).

[14]J. Fousek and V. Janovek, J. Appl. Phys. **30**, 135 (1969).

[15]J. Sapriel, Phys. Rev. B **12**, 5128 (1975).

[16]V. Janovek, Ferroelectrics **35**, 105 (1981).

[17]R. Portier and D. Gratias, J. Phys. (Paris) Colloq. **43**, C4-17 (1982).

[18]S. R. Andrews and R. A. Cowley, J. Phys. C **19**, 615 (1986).

[19]L. Landau and E. Lifshitz, Phys. Z. Sowjetunion **8**, 153 (1935).

[20]V. A. Zhirnov, Zh. Eksp. Teor. Fiz. **35**, 1175 (1958) [Sov. Phys.—JETP **35**, 822 (1959)].

[21]L. N. Bulaevskii and V. L. Ginzburg, Zh. Eksp. Teor. Fiz. **45**, 772 (1963) [Sov. Phys.—JETP **18**, 530 (1964)]; L. N. Bulaevskii, Fiz. Tverd. Tela (Leningrad) **5**, 3183 (1963) [Sov. Phys.—Solid State **5**, 2329 (1964)].

[22]A. Fousková and J. Fousek, Phys. Status Solidi A **32**, 213 (1975).

[23]Y. Ishibashi and V. Dvôrák, J. Phys. Soc. Jpn. **41**, 1650 (1976).

[24]B. Capelle and C. Malgrange, J. Phys. (Paris) **45**, 1827 (1984).

[25]G. R. Barsch and J. A. Krumhansl, in *Proceedings of the International Conference on Solitons on Real Systems,* edited by J. A. Fernandez and G. Reinish (Centre Universitaire Mediterraneen, Nice, 1982), p. 90; Phys. Rev. Lett. **53**, 1069 (1984).

[26]F. Falk, Z. Phys. B **51**, 177 (1983).

[27]A. E. Jacobs, Phys. Rev. B **31**, 5984 (1985).

[28]G. R. Barsch, W. Cao, and J. A. Krumhansl (unpublished).

[29]S. W. Meeks, B. A. Auld, P. Maccagno, and A. Miller, Ferroelectrics **50**, 571 (1983).

[30]S. W. Meeks and B. A. Auld, in *1983 IEEE Ultrasonics Symposium Proceedings,* edited by B. R. McAvoy (IEEE, Piscataway, 1983), p. 535.

[31]G. R. Barsch, B. Horovitz, and J. A. Krumhansl, Phys. Rev. Lett. **59**, 1251 (1987).

[32]B. Horovitz, G. R. Barsch, and J. A. Krumhansl, Phys. Rev. **36**, 8895 (1987).

[33]C. H. Chen, D. J. Werder, S. H. Liou, J. R. Kwo, and M. Hong, Phys. Rev. B **35**, 8767 (1987).

[34]M. Hervieu, B. Domenges, C. Michel, G. Heger, J. Provost, and B. Raveau, Phys. Rev. B **36**, 3920 (1987).

[35]J. L. Hodeau, C. Chaillout, J. J. Capponi, and M. Marezio, Solid State Commun. **64**, 1349 (1987).

[36]R. M. Fleming, B. Batlogg, R. J. Cava, and E. A. Rietman, Phys. Rev. B **35**, 7191 (1987).

[37]I. K. Schuller, D. G. Hinks, M. A. Beno, D. W. Capone II, L. Soderholm, J. P. Locquet, Y. Bruenseraede, C. U. Segre, and K. Zhang, Solid State Commun. **63**, 385 (1987).

[38]R. J. Birgeneau, C. Y. Chen, D. R. Gabbe, H. P. Jenssen, M. A. Kastner, C. J. Peters, P. J. Picone, T. Thio, T. R. Thurston, and H. L. Tuller, Phys. Rev. Lett. **59**, 1329 (1987).

[39]J. D. Jorgensen, M. A. Beno, D. G. Hinks, L. Soderholm, K. J. Volin, R. L. Hitterman, J. D. Grace, I. K. Schuller, C. U. Segre, K. Zhang, and M. S. Kleefisch, Phys. Rev. B **36**, 3608 (1987).

[40]D. deFontaine, L. T. Wille, and S. C. Moss, Phys. Rev. B **36**, 5709 (1987).

[41]C. Varea and A. Robledo, Int. J. Mod. Phys. B **2**, 763 (1988).

[42]E. A. H. Love, *A Treatise on the Mathematical Theory of Elasticity* (Dover, New York, 1944), p. 49.

[43]Note that because of the symmetry of the strain tensor ($\eta_{ij}=\eta_{ji}$) for $i\neq j$ a factor $\frac{1}{2}$ arises, i.e., it is $H_{rs2}=-1/\sqrt{2}$, $H_{3s4}=1/\sqrt{2}$, etc.

[44]W. Cao, Ph.D. thesis, The Pennsylvania State University, 1987.

[45]B. Alefield, Z. Phys. **222**, 155 (1969).

[46]R. O. Bell and G. Rupprecht, Phys. Rev. **129**, 90 (1963).

[47]V. J. Minkiewicz, Y. Fujii, and Y. Yamada, J. Phys. Soc. Jpn. **28**, 443 (1970).

[48]G. Sorge, G. Schmidt, F. Hegenbarth, and C. Frenzel, Phys. Status Solidi **37**, K17 (1972).

[49]B. Okai and J. Yoshimoto, J. Phys. Soc. Jpn. **39**, 162 (1975).

[50]W. Rehwald, Phys. Kondens. Materie **14**, 21 (1971).

[51]E. Pytte, in *Structural Phase Transitions and Soft Modes,* edited by E. J. Samuelsen, E. Andersen, and J. Feder (Universitätsforlaget, Oslo, 1971), p. 151.

[52]W. G. Stirling, J. Phys. C **5**, 2711 (1972).

[53]G. R. Barsch and J. A. Krumhansl, Met. Trans. **19A**, 761 (1988); G. R. Barsch, W. Cao, and J. A. Krumhansl, Solid State Commun. (to be published).

[54]O. Muller and R. Roy, *The Major Ternary Structural Families* (Springer, Berlin, 1974), p. 175.

[55]R. A. Cowley, Phys. Rev. A **134**, 981 (1964).

[56]W. Cao and G. R. Barsch (unpublished).

[57]J. Lajzerowicz, Ferroelectrics **35**, 219 (1981).

[58]H. T. Davis, *Introduction to Nonlinear Differential and Integral Equations* (Dover, New York, 1962), Chap. 6.

[59]S. Aubry, J. Chem. Phys. **62**, 3217 (1975); **64**, 3392 (1976).

[60]Y. Ishibashi and I. Suzuki, J. Phys. Soc. Jpn. **53**, 4250 (1984).

[61]E. Pytte and J. Feder, Phys. Rev. **187**, 1077 (1969); J. Feder and E. Pytte, Phys. Rev. B **1**, 4803 (1970).

[62]K. Binder, in *Phase Transitions and Critical Phenomena,* edited by C. Domb and J. L. Lebowitz (Academic, New York, 1983), Vol. 8, p. 1.

[63]K. Gesi, J. D. Axe, G. Shirane, and A. Linz, Phys. Rev. B **5**, 1933 (1972).

[64]L. P. Bouckaert, R. Smoluchowski, and E. Wigner, Phys. Rev. **50**, 58 (1936).